Active control of boundary layer instabilities using MEM's

Active control of boundary layer instabilities using MEMs

Second Traineeship 2002
Rep. No. 2002.69

J.D.B.J. van den Boom, s440881

Supervisor (Queen Mary, University of London): Dr. H.J.C. Huijberts
Supervisor (Technische Universiteit Eindhoven): Prof. Dr. H. Nijmeijer

November 2002

Contents

Nomenclature

symbol	description	unit
A, B, C, D	state variable form in matrix notation	
A_c, B_c, C_c, D_c	state variable form of controller	
$C(s)$	transfer function for controller	
d	disturbance	
F	Frequency number	
$G(s), H(s), T_{zw}(s)$	transfer function	
i	complex number	
K	value for proportional controller, gain	
P	pressure of mean flow	Pa
p	pressure	Pa
R_e	Reynolds number	
r	reference signal	
s	complex number	
t	time	s
U	mean velocity in x-direction	m/s
U_m	maximum velocity main flow	m/s
u	velocity in x-direction	m/s
u	control signal	
V	mean velocity in y-direction	m/s
v	velocity in y-direction	m/s
v	control input	
$W(s)$	transfer function for weight filter	
w	exogenous input	
x	(horizontal) position	m
y	(vertical) position	m
y	plant output	
z	exogenous output	

symbol	description	units
$\mathsf{Re}(\alpha)$	streamwise wavenumber	
$\mathsf{Im}(\alpha)$	degree of amplification or damping	
γ	(upper)bound for ∞-norm	
δ	height of boundary layer	m
ζ	damping ratio	
η	measurement noise	
μ	dynamical viscosity	kg/(ms)
ρ	density	kg/m^3
$\bar{\sigma}$	maximal singular value	
τ	time delay	s
τ_w	skin friction	N/m^2
υ	kinematic viscosity	m^2/s
$\phi_a(y)$	amplitude function	
$\phi(\omega)$	phase	[°]
$\psi(x,y,t)$	streamfunction	
ω	angular frequency	rad/s
ω_n	undamped natural frequency	rad/s

Preface

This report is the result of my traineeship at Queen Mary, University of London to investigate active control of boundary layer instabilities with an emphasis on closed-loop control. The area of flow control plainly resides at the intersection of disciplines, incorporating essential and nontrivial elements from control theory, fluid mechanics, Navier-Stokes mathematics, and numerical methods. I started this traineeship knowing little about the magical world of fluid dynamics. I found out that this world is (very) large and intriguing. I hope that what I have written explains feedback control to the aeronautical reader while at the same time providing background on the theory of transition from laminar to turbulent flow to the interested control engineer.

I want to thank Prof. M. Gaster, the big promoter behind the research, and Yong Li, the Ph.D. student I was working with. After some language-problems during the first weeks we started to understand each other better. He helped me to understand this little part of flow concerning my traineeship. I hope I have triggered him (I know for sure) to do some research or experiments about closed-loop control.

I would like to express my gratitude to my new friends Dr. Krishna Singh, Emanuel Caloupis, Yak Sing, Laureen McFarlane, Yujiong Cheng, Ernesto Pinto, Gerardo Vasquez-Gomez and all other persons who made my stay in London a time not to forget. I want to thank my landlord and "roommate" Kit Niaz (and his girlfriend Saba) for allowing me to stay in his house.

My special thanks go to Dr. H.J.C. Huijberts, who made this project possible and was always willing to help me with the problems during this project. He was also responsible for given me a job as a demonstrator of a second-year lab about control systems. Demonstrating this lab was a great experience, it thaught me how to explain everything clearly and it thaught me how the English university system works.

Chapter 1

Introduction

On the wing of an aircraft transition from a laminar to a turbulent boundary layer generally occurs through the amplification of naturally excited instability waves. An aircraft wing encounters a free-stream environment that is reasonably clean. Nevertheless, it will contain weak acoustic and vorticity fluctuations that can initiate disturbances in the boundary layer, especially when there are small roughness elements or disturbances in the surface.

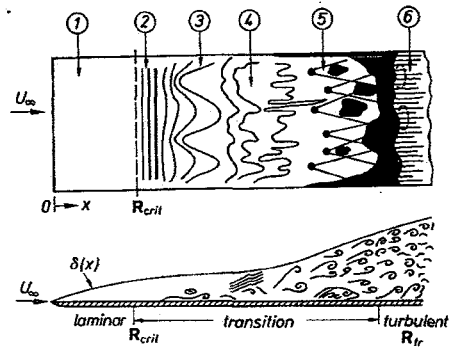

Figure 1.1: Transition in the boundary layer on a flate plate

The process of transition in the boundary layer on a flat plate in the presence of an external flow (of low turbulence intensity) is shown in Figure 1.1. The flow goes through the following stages, starting with the leading edge.

1. Stable laminar flow following the leading edge;
2. Unstable laminar flow with two-dimensional Tollmien-Schlichting[1] waves;
3. Development of unstable, laminar, three-dimensional waves and vortex formation;

[1]Very small two-dimensional type disturbances that may induce transition to turbulent flow-named after German aerodynamicists Walter Tollmien and Hermann Schlichting.

4. Burst of turbulence in places of very high local vorticity;
5. Formation of turbulent spots in places where the turbulent velocity fluctuations are large;
6. Coalescence of turbulent spots into a fully developed turbulent boundary layer.

A fluid flowing past a body will exert normal and tangential stresses on the surface. Normal stresses (pressure) can be measured using a manometer. Measurement of the shear or tangential stress is more difficult. The knowledge of the variation of the wall shear stress (skin friction) is useful in analyzing a flow field, because a turbulent boundary layer has considerably larger skin-friction than a laminar flow. Skin friction (τ_w) is defined as:

$$\tau_w = \mu \frac{\partial U(x,y)}{\partial y} \tag{1.1}$$

where μ is the viscosity (constant) and $\frac{\partial U}{\partial y}$ is the gradient of the streamwise velocity.

The friction will be measured using thermal anemometry. Thermal anemometers measure the fluid velocity by sensing changes in heat transfer from a sensor to the motion of the fluid. The sensors are in general small and have a good frequency response which make them suitable for studying flow details. Examples of thermal anemometers are hot-film and hot-wire sensors.

Reduction of drag produced by skin friction, or, in other words, reduction of wall shear stresses generated by (near-wall) turbulence has received a lot of attention. The skin friction constitutes respectively about 50%, 90% and 100% of the total drag on commercial aircraft, underwater vehicles and pipelines, [21]. It is important, in a design sense, to be able to predict the position of the transition. (This estimates the losses or drag). It would even be more beneficial if the transition process could be controlled.

Examples of passive control for delaying the transition are motion of the solid wall, acceleration of the boundary layer (blowing), suction, injection of a different gas (binary boundary layers), provision of suitable shapes (laminar airfoils) and cooling the wall. The effect of suction consists in the removal of fluid particles from the boundary layer. This makes it possible to shift the point of transition in the boundary layer in downstream direction. This delay reduces the boundary-layer thickness which then becomes less prone to turning turbulent. Cooling (or heating) the wall will also reduce the thickness of the boundary layer.

To interfere actively with the laminar-turbulent transition is not a new thought. This is an on-going project at Queen Mary, University of London. Professor M. Gaster is the great "promoter" behind this project.

The general layout of the experiment is sketched in Figure 1.2. A rigid flat plate with a sharp edge is mounted in a closed-loop windtunnel[2]. The walls of the tunnel are far enough apart to be of insignificant influence. The incoming stream of air has a low turbulence level and a constant velocity U. Along the useful side of the plate a boundary layer will develop to a thickness. Normally, the layer begins to oscillate without any external prompting, and

[2] In these kind of windtunnels the air, used for testing, circulates.

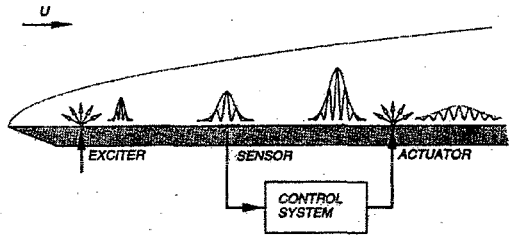

Figure 1.2: Experimental (control) setup

it becomes turbulent at some distance from the leading edge. To mimic the receptivity process and because the free-stream turbulence in the windtunnel was low it was necessary to introduce controlled disturbances. By creating these disturbances artificially there is complete control of the wave field. The artificial oscillation will outgrow the natural waves and can be easily observed. The artificial perturbation is produced by an exciter. The exciter is a point source (a loudspeaker has commonly been utilized for studies of localized disturbances). The acoustic pulse is injected through a small hole. The use of a loudspeaker makes it possible to excite the flow harmonically or with deterministic white noise. The amplitude and frequency of the pulse can be regulated. The skin friction is then measured by a sensor (hot-wire anemometer). This makes it possible to derive a value for the velocity-components of the air stream. This signal of the sensor is evaluated for any given source signal by a convolution with the impulse response. Similarly, the far field, which has to be cancelled, could be obtained by convolution of the input excitation and the impulse response to a downstream position where the effectiveness of the control is to be assessed. The driving signal, fed to the control actuators, is found using the inverse of the impulse response. (Only using the unstable eigen-solution, see Chapter 2).

For this method of (feedforward) controlled wave-cancellation, it is required to know the content of the oncoming wave-field. This content is derived experimentally. This is compared with numerical results. The resemblance will not be 100%, because of model errors and electrical noise. It would be better to use closed-loop control. The "powers" of closed-loop control are that it is able to cope with unknown disturbances and model errors. Since the control problem involves the attenuation of disturbances (wave-cancellation) it seems obvious to use feedback control. The objective of this project is to investigate if closed loop control is conceivable and if it is possible implement it numerically.

In Chapter 2 a deeper insight is given in laminar-turbulent transition, especially on the stability theorem. A workable model will be derived in Chapter 3 for the instability waves using transfer function analysis. With this model it will be possible to build a closed-loop controller for disturbance attenuation. This is first done using a classical approach in Chapter 4 (only a proportional controller) and in Chapter 5 using robust control techniques ($\mathcal{H}_\infty$-control). Finally conclusions will be drawn in Chapter 6.

Chapter 2

Stability theory of a laminar flow

The transition from a laminar to a turbulent flow is still not fully understood. Theoretical investigations are based on the assumption that laminar flows are affected by small disturbances. When disturbances decay with time the main flow is considered stable. On the other hand the main flow is unstable when disturbances increase with time and there is the possibility of transition to turbulence. This theory of stability for laminar flows decomposes motion into a mean flow and a superimposed disturbance.

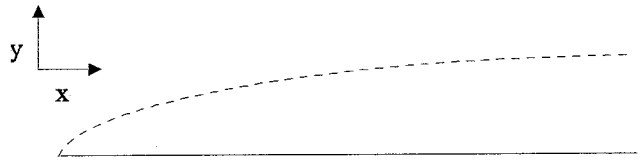

Figure 2.1: General Configuration

The general configuration for a flat plate is given in Figure 2.1, where the boundary layer height has been sketched in dashed lines. The x-coordinate represent the streamwise position and the y-coordinate the height of the boundary layer. Only a two-dimensional description for the transition process is investigated here (two-dimensional mean flow and a two-dimensional disturbance). The steady and incompressible mean flow is described by the Cartesian velocity components U and V. The pressure of the mean flow is expressed by P. The quantities for the non-steady disturbance (small compared to the mean flow) are denoted as u', v' and p'. The resultant motion has the velocity components:

$$u = U + u';\ v = V + v' \tag{2.1}$$

and the pressure component:

$$p = P + p' \tag{2.2}$$

In the theoretical treatment of instability waves it is often convenient to ignore the fact that the boundary layer increases in thickness with downstream distance. This approximation (parallel flow) implies that the mean flow velocity U only depends on y and V is supposed to be zero. The pressure in the mean flow has a dependency on x as well as on y.

$$U = U(y);\ V = 0;\ P = P(x, y) \tag{2.3}$$

The two-dimensional perturbations are a function of time (t) and space (x, y). Its velocity and pressure components are:

$$u'(x, y, t);\ v'(x, y, t);\ p'(x, y, t) \tag{2.4}$$

Assuming that the mean flow is a solution of the Navier-Stokes equation[1], the resultant motion must also satisfy the Navier-Stokes equation. This makes it possible to obtain three equations for u', v' and p'.

$$\frac{\partial u'}{\partial t} + U\frac{\partial u'}{\partial x} + v'\frac{\partial U}{\partial y} + \frac{1}{\rho}\frac{\partial p'}{\partial x} = \nu(\nabla^2 u') \tag{2.5}$$

$$\frac{\partial v'}{\partial t} + U\frac{\partial v'}{\partial y} + \frac{1}{\rho}\frac{\partial p'}{\partial y} = \nu(\nabla^2 v') \tag{2.6}$$

$$\frac{\partial u'}{\partial x} + \frac{\partial v'}{\partial y} = 0 \tag{2.7}$$

where ρ is the density and ν is the kinematical viscosity.

The boundary conditions specify that the velocity components u' and v' vanish on the wall (no-slip condition). The pressure p' can be eliminated from the equations (2.5) and (2.6).

A stream function, $\psi(x, y, t)$, representing a single oscillation of the disturbance, which is composed of a number discrete partial fluctuations, each of which is said to consist of a wave which is propagated in the x-direction, is introduced. Any arbitrary two-dimensional disturbance is expanded in a Fourier series. The stream function is of the form:

$$\psi(x, y, t) = \phi_a(y)e^{i(\alpha x - \omega t)} \tag{2.8}$$

where $\phi_a(y)$ is an amplitude function. This function depends only on y because the mean flow depends on y only. α is a complex value. The real part, $\mathsf{Re}\,(\alpha)$, is the streamwise wave-number and the imaginary part, $\mathsf{Im}\,(\alpha)$, determines the degree of amplification (<0) (or damping (>0)). ω is the angular frequency of oscillation. The components of the perturbation velocity are obtained from (2.8):

$$u' = \frac{\partial \psi}{\partial y} = \phi_a'(y)e^{i(\alpha x - \omega t)} \tag{2.9}$$

[1] The assumed form of the mean flow, equation (2.3), can be criticised on the ground that the variation of the component U of the velocity with x as well as the normal component V have been neglected.

$$v' = -\frac{\partial \psi}{\partial x} = -i\alpha R_e \phi_a(y) e^{i(\alpha x - \omega t)} \tag{2.10}$$

where R_e is the (dimensionless) Reynolds number, defined as $R_e = \frac{U_m \delta}{\nu}$. U_m is the maximum velocity of the main flow and δ is the boundary-layer thickness.

Introducing the expressions (2.9) and (2.10) in the simplified Navier-Stokes equations (2.5,2.6) and the equation of continuity (2.7) the following ordinary fourth-order differential equation for the amplitude $\phi(y)$ is obtained:

$$(U - \frac{\omega}{\alpha})(\ddot{\phi} - \alpha^2\phi) - \ddot{U}\phi = -\frac{i}{\alpha R_e}(\phi^{(4)} - 2\alpha^2\phi + a^4\phi) \tag{2.11}$$

This differential equation (2.11), commonly referred to as the Orr-Sommerfeld equation, forms the point of departure for the stability theorem of laminar flow [22].

2.1 Solution of the Orr-Sommerfeld Equation

The determination of the stability of any given system involves nothing more than the solutions of this the Orr-Sommerfeld Equation (2.11) combined with the boundary conditions given for the (particular) flow. The boundary conditions are (perturbation velocity must vanish at the wall and at large distance (free stream)):

$$\begin{aligned} y &= 0 : u' = v' = 0 : \phi = 0 : \phi' = 0 \\ y &= \infty : u' = v' = 0 : \phi = 0 : \phi' = 0 \end{aligned}$$

In general, a differential equation, such as that of Orr-Sommerfeld (2.11), which is constrained by sufficient boundary conditions, admits an infinite but discrete set of solutions. Each solution is called a mode (or eigenfunction) and has a particular corresponding eigenvalue. Once this information has been obtained, the salient output become the eigenvalues, ω the angular frequency of oscillation, as a function of the wave-number $\mathrm{Re}\,(\alpha)$, and the Reynolds number, R_e.

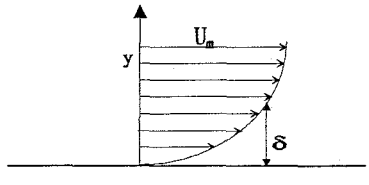

Figure 2.2: Velocity profile

To solve the eigenvalue problem the mean flow *U(y)* has been specified with a mean velocity profile, Figure 2.2. The Reynolds number of the mean flow is specified with the choice for the mean flow. The frequency of the partial oscillation, a real number, is chosen. The initial value for the eigenvalue α (complex), α^*, is guessed. The problem is then solved from the outer boundary conditions marching to the plate-boundary using a shooting method and 4^{th} order Runge-Kutta algorithm. The shooting method incorporates a manner of eliminating

the parasitic growth that arises with stiff high Reynolds number equations. At the end of each integration step all the solution variables and their derivatives are defined. These can be combined together in any convenient way to remove parasitic growing solutions (scaling), providing new variables for the next integration step. This process of stepwise integration and filtering is continued to the wall where the remaining boundary condition is applied. If the choice of the wavenumber is compatible with an eigenmode of the system the remaining velocity component becomes zero. An iteration scheme can be set up to vary the wavenumber or frequency parameter until all the velocity components become zero at the boundary. (If the solution at the plate is the same as the boundary condition value at the plate the guess for α^* is good. The eigen-solution has been found. If the solution at the wall is not the same, α^* is perturbed with $\triangle\alpha$ and the problem is solved again (and again) to reach a feasible solution. (For every α a unique solution can be found)). The eigenfunction can be readily constructed from the previously stored scaling factors.

Singularity of the integrand(s), which give a solution to the Orr-Sommerfeld equation, is also a problem. The integral(s) can be evaluated by carrying out an appropriate contour integration using quite small steps close to the singularity. This turns out to be both inconvenient to implement and very expensive in computational effort. Also this approach does not enable a simple Fourier series representation of the solution to be found. Since this is expected as a physical solution when the flow is excited by a disturbance that generates Tollmien-Schlichting modes it is necessary to condition the integrand(s) in some way so as to remove the singular character from the integrand(s).

A method is to substract the singularity from the integrand(s) and treating the singular part of the inversion analytically. This approach is useful because it separates out the near-field features of the solution and the far field eigen-solution. The near-field features have their influence close to the actuator, both in upstream ($-x$) and downstream ($+x$) direction. The influence of the eigen-solution takes only place in the downstream direction.

The eigen-solution is the Orr-Sommerfeld part of the solution obtained for a strictly parallel flow which will only be useful close to the source. The appropriate eigen-solution for weakly nonparallel flows can be computed without too much difficulty and used to replace this term. In this way it should be possible to construct solutions that are valid over the whole of the physical plane. The separation in (unstable) eigen-solutions and a near-field part of the solution is essential for the control problem as it is only the far field, that has to be cancelled, [b11].

It is possible to study stability for a given mean velocity profile graphically in a (F, R_e)-diagram, (Figure 2.3)[2]. The (dimensionless) Frequency number (F) is defined as $\frac{\omega\nu}{U_m^2}$. Wave disturbances can either be considered to evolve in time or in space and the corresponding stability problems are known as the temporal or the spatial problem. Here only the spatial problem is solved for the complex wavenumber α and the angular velocity is a real parameter. The temporal problem would be solved for a complex ω and α appearing as a real parameter. Every point in the (F, R_e)-diagram corresponds to a pair of values of $\mathsf{Re}(\alpha)$ and $\mathsf{Im}(\alpha)$. The locus $\mathsf{Im}(\alpha) = 0$ will separate the region of stable and unstable disturbances. This locus is called the curve of neutral stability.

[2] Figure based on measurements preformed by Ph.D.-student Yak Sing

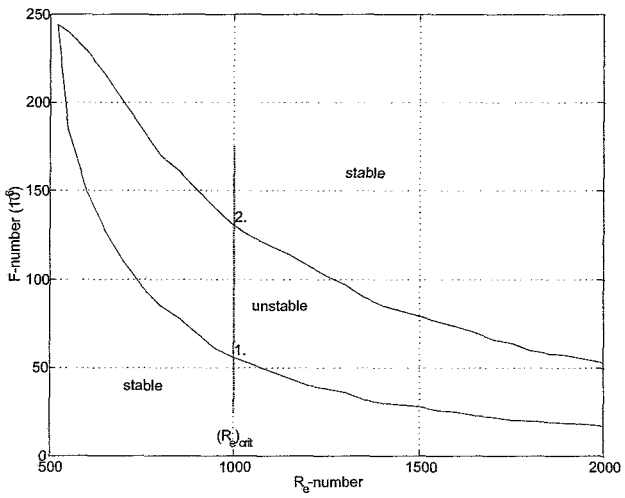

Figure 2.3: Curve of neutral stability boundary layer

The point on this curve at which the Reynolds number has its smallest value (parallel to the F-axis) is of greatest interest since it indicates that value of the Reynolds number below which all individual oscillations decay, whereas above that value at least some are amplified. The smallest Reynolds number is called the critical Reynolds number or limit of stability with respect to the laminar flow under consideration. It is necessary to remark at this point that the critical Reynolds number calculated from stability considerations cannot be expected to be equal to the Reynolds number observed at the point of transition. The distance between the point of instability and point of transition depends on the degree of amplification.

The mean flow used during this project has a critical Reynolds number of 1000 on the point of excitation. A vertical line, at $R_{e_{crit}} = 1000$, is drawn in Figure 2.3. This line intersects the locus at two points. At point 1. the F-number is $56 \cdot 10^{-6}$ and at point 2. the F-number is $130 \cdot 10^{-6}$ ($U_m = 10.3$ [m/s] and $\nu = 1.48 \cdot 10^{-5}$ [m^2/s] (For air with pressure of 0.099 [MPa] and temperature of 293 [K])). In the first case the angular frequency will be 314.159 [rad/s] and in the second case 942.477 [rad/s]. The working range of the controller has to be between these values because there is no value in trying to cancel stable eigen-solutions.

Chapter 3

Transfer function analysis

A transfer function of a system $H(s)$ can be described in the frequency domain by the relation (let $s = i\omega$) :

$$H(i\omega) = \mathsf{Re}(H(j\omega)) + i\,\mathsf{Im}(H(i\omega)) \tag{3.1}$$

Alternatively, the transfer function can be represented by a magnitude $|H(i\omega)|$ and a phase $\phi(i\omega)$ as

$$H(i\omega) = |H(i\omega)|\, e^{i\phi(i\omega)} \tag{3.2}$$

where

$$|H(\omega)|^2 = (\mathsf{Re}(H(i\omega)))^2 + (\mathsf{Im}(H(i\omega)))^2 \tag{3.3}$$

$$\phi(\omega) = \arctan\left(\frac{\mathsf{Im}(H(i\omega))}{\mathsf{Re}(H(i\omega))}\right) \tag{3.4}$$

In situations where the transfer function of a system is unknown, the Bode diagram is of great value. The frequency response data are obtained experimentally in the frequency range of interest. In order to interpret the Bode diagrams one usually takes logarithmic scales on ω-axis and plots $20\log_{10}|H(\omega)|$ to get units in [dB]. The system transfer function is derived within a certain degree of accuracy by fitting an asymptotic log-magnitude plot to the experimental data. The procedure is outlined below:

1. The experimental data (real and imaginary part of $H(i\omega)$) is used to plot the exact (log)-magnitude versus frequency curves on semilog graph sheet;

2. Asymptotes are then drawn on the (log)-magnitude curve keeping in mind that the slopes of the asymptotes must be multiples of ± 20 [dB/decade]. The break frequency (or corner frequency) is so adjusted that the dB value at the break frequency on the asymptotic plot differs from the actual (log)-magnitude plot which is in close agreement with the dB-correction of the kind of factor revealed;

3. Suppose that the slope of asymptotic (log)-magnitude curve acquired in 2)., changes by $-20m$ [dB/decade] (m = multiple, integer) at $\omega = \omega_1$, indicates the presence of the factor $\frac{1}{(1+\frac{i\omega}{\omega_1})^m}$ in the transfer function. The change of slope by -40 [dB/decade] reveals that either a double pole ($m = 2$) or a pair of complex poles is present. If the error between the asymptotic and the actual curve is about -6 dB then a factor of the form $\frac{1}{(1+\frac{i\omega}{\omega_1})^2}$ exists in the transfer function and if the error is positive then a quadratic factor of the form $\frac{1}{(1+2i\zeta(\frac{\omega}{\omega_1})+(\frac{\omega}{\omega_1}))^2}$ is present. The difference between the actual (log)-magnitude curve and the asymptotic approximation is a function of the damping ratio ζ and must be accounted for when $\zeta < \frac{1}{2}\sqrt{2}$;

4. If the slope changes by $20m$ [dB/decade] at $\omega = \omega_2$, this indicates a factor $(1 + \frac{i\omega}{\omega_2})^m$ in the transfer function;

5. In the low frequency range, the plot is controlled by a factor of the form: $\frac{K}{(i\omega)^r}$. In most practical cases r equals 0,1 or 2. The value for r is determined as follows:

   - If the low frequency asymptote is a horizontal at x [dB], it indicates that the transfer function represents a type-0 system with a gain K given by $20\log_{10}(K) = x$;
   - If the low frequency asymptote has a slope of -20 [dB/decade], it denotes the presence of a factor of the form $\frac{K}{i\omega}$ in the transfer function. The frequency at which the (extended if necessary) asymptote intersects the 0-dB line numerically represents the value of K;
   - If the low frequency asymptote has a slope of -40 [dB/decade], then the transfer function has a factor of the form $\frac{K}{(i\omega)^2}$. The frequency at which this asymptote (extended if necessary) intersects the 0-dB line is numerically equal to $\sqrt{K}$.

After obtaining the transfer function from the (log)-magnitude curve, the real and imaginary part of the experimentally (or numerically) obtained and approximated transfer function are compared. If there is a poor comparison it is possible due to the presence of time-delay. A pure time delay, without attenuation, is represented by the transfer function: $H_d(s) = e^{-s\tau}$, where τ is the delay time. The delay adds a phase shift to the frequency response without changing the (log)-magnitude curve. The factor does not introduce any additional poles or zeros. Known is:

$$\phi(\omega) = -\omega\tau \tag{3.5}$$

When expression (3.5) is used it is possible to derive an expression for τ:

$$\tau = -\frac{1}{\omega}\arctan\left(\frac{\mathrm{Im}(H(j\omega))}{\mathrm{Re}(H(j\omega))}\right) \tag{3.6}$$

The maximum value for the time-delay can be found at the frequency where the quotient of the real and imaginary part has its absolute maximum.

3.1 Models for the eigen- and nearfield-solution

Ph.D.-student Y. Li has generated the data by solving the Orr-Sommerfeld equation (2.11) for 50 frequencies between 0 and 3141.593 [rad/s] and 251 x-positions between -50 (upstream) and 200 [mm] (downstream) using a computer code in *Fortran*. The generated data have been the real and imaginary part of the solutions. Equation (3.3) makes it possible to construct a magnitude-plot. The following figures give a representation of the eigen-solution (3.1) and the nearfield down-(3.2) and upstream(3.3) for different values of x. Probably

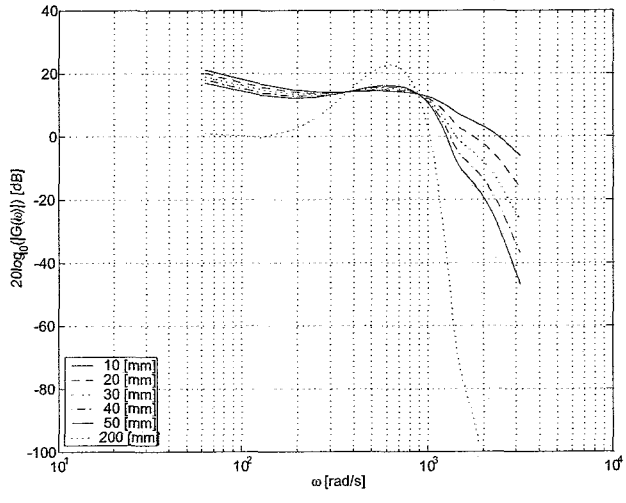

Figure 3.1: Magnitude for different values of x (eigen-solution)

the amplification or damping of the transfer functions is caused by a changing distance. Using the described method it was not possible to get a good resemblance. It seems that lines with a slope of ± 10 [dB/decade] fit better on both the nearfield solutions. There are similarities between the theory for stability in boundary layers and heat transfer. In *Loiseau et al.* [15] a transfer function for a heat transfer problem (heat conducting rod) is derived using $\sqrt{s}$ in the transfer function. Models described by square roots in their transfer function are often referred to as fractional systems. Therefore the procedure outlined above is extended with the following steps:

1. Suppose that the slope of asymptotic (log-)magnitude curve acquired in changes by -10 [dB/decade] at $\omega = \omega_1$, indicates the presence of the factor $\frac{1}{\sqrt{(1+\frac{i\omega}{\omega_1})}}$ in the transfer function;

2. Suppose that the slope of asymptotic (log-)magnitude curve acquired in changes by -10 [dB/decade] at $\omega = \omega_1$, indicates the presence of the factor $\sqrt{(1+\frac{i\omega}{\omega_1})}$ in the transfer function.

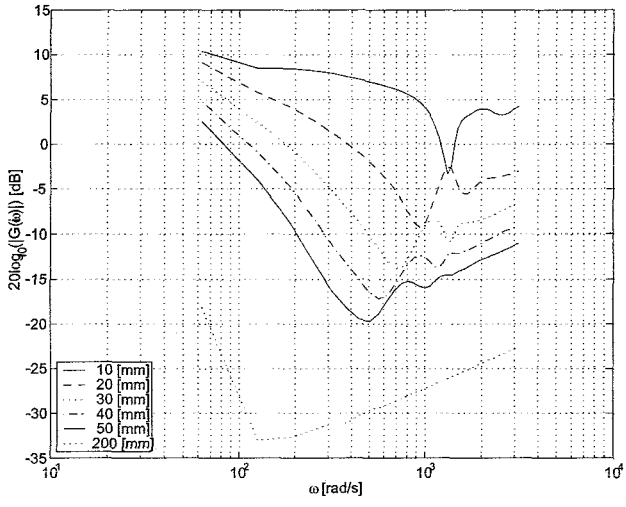

Figure 3.2: Magnitude for different values of x (downstream)

- If the low frequency asymptote has a slope of -10 [dB/decade], it denotes the presence of a factor of the form $\frac{K}{\sqrt{i\omega}}$ in the transfer function. The frequency at which the (extended if necessary) asymptote intersects the 0-dB line numerically represents the value of K;

The transfer functions are derived for a distance of -20 [mm] (upstream) and 20 [mm] (downstream) (Figures 3.4, 3.5 and 3.6). The models for the eigen-solution and both the nearfield solutions are:

$$G^{eigen}(s) = \frac{4.87e^{-0.0028s}}{(s/900)^2 + 1.035(s/900) + 1} \tag{3.7}$$

$$G^{near}_{up}(s) = \frac{\sqrt{s + 100}}{s} \tag{3.8}$$

$$G^{near}_{down}(s) = \frac{22\sqrt{s/1000 + 1}e^{-0.0024s}}{\sqrt{s}\left((s/1000)^2 + 0.4\,(s/1000) + 1\right)} \tag{3.9}$$

It is expected that at a distance of 20 [mm] no feedback of the upstream near-field-solution from the actuator to the sensor occurs. (In the feedforward control case this could cause the control loop to become unstable.) Therefore (3.9) will be neglected in further investigation.

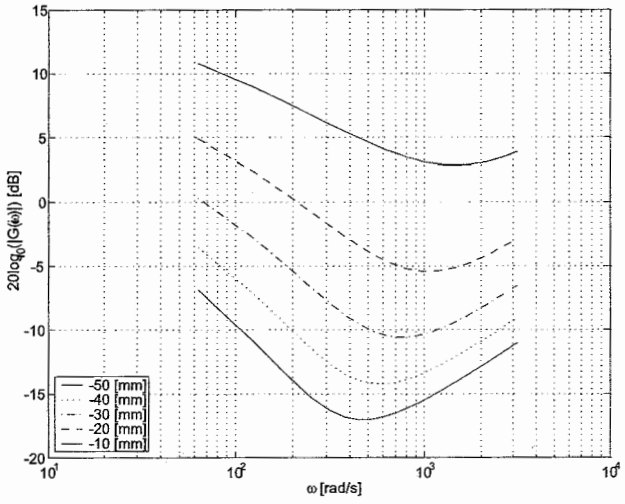

Figure 3.3: Magnitude for different values of x (upstream)

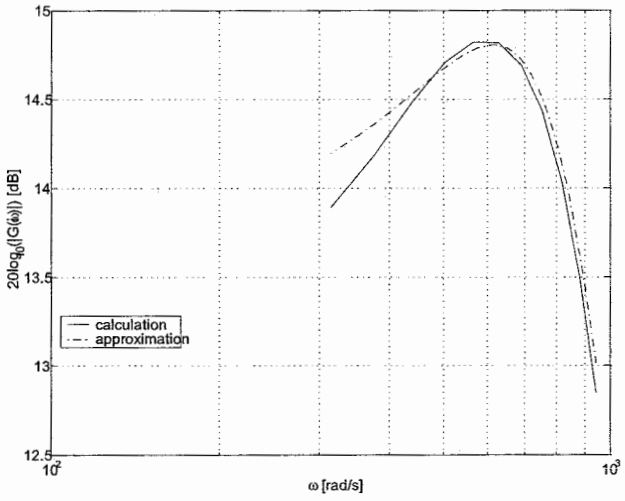

Figure 3.4: Eigen-solution

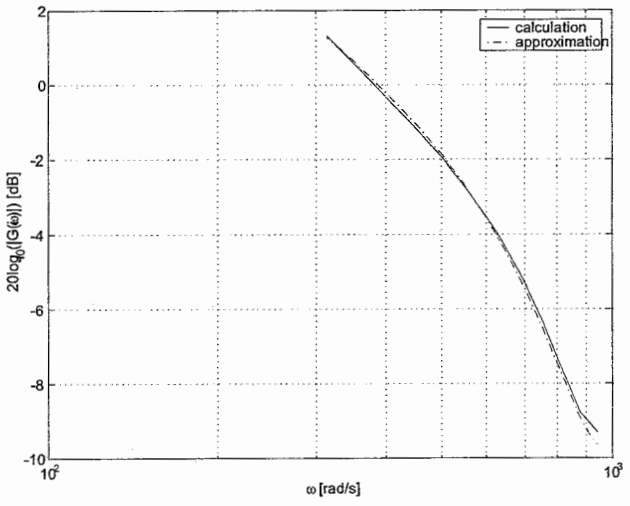

Figure 3.5: Nearfield solution (downstream)

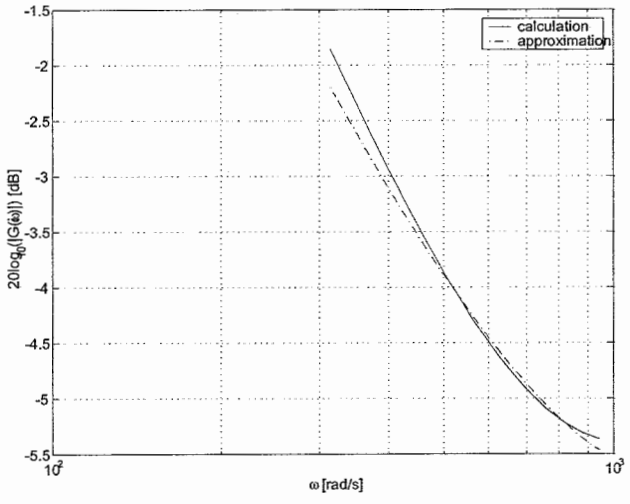

Figure 3.6: Nearfield solution (upstream)

Chapter 4

Classical Control

The model which describes the behaviour of the flow in the boundary layer due to an external disturbance is now known, so it is time to construct a controller. The control aim is to decrease the effect of the perturbation d on the wave y over a certain frequency range. The block diagram, given in Figure 4.1, is slightly different from the actual to be controlled system. The scheme is used to introduce some variables/ parameters.

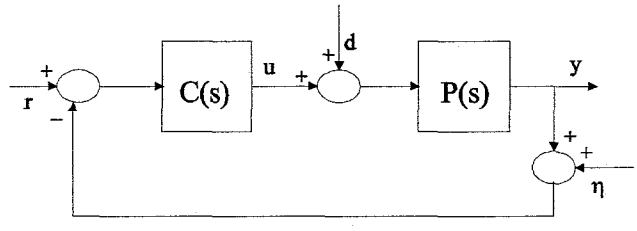

Figure 4.1: Block diagram used to introduce variables/ parameters

The (exogenous) inputs consist in this case of the reference signal r, the disturbance d and the measurement noise η. $C(s)$ is the controller and $P(s)$ describes the behaviour of the flow to which control has to be applied. y is the output and u the control signal. The plant includes the actuator. The sensor noise will be explicit in η. In general the sensor has a transfer function different from 1, so an extra block in the feedback scheme should be inserted just before the addition of the sensor noise. However, good quality sensors have a flat frequency response for a much broader band than the process transfer. If this is the case the transfer function may be neglected. Since our goal is disturbance attenuation the reference will be set to zero just as the measurement noise, assuming perfect measurement. The feedback scheme will then have the structure in Figure 4.2.

In the design of the feedforward controller only the eigen-solution is used to build a controller. Measuring the skin friction will give no separate information about the eigen- and nearfield solution. So it would be convenient to build a

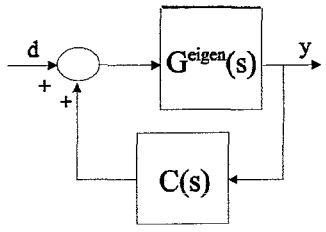

Figure 4.2: Feedback diagram for the eigen-solution

controller based on both transfer functions. The upstream nearfield solution will not be considered, because the transfer functions are derived on a distance of 20 [mm] between the sensor and the actuator. This distance should be sufficient to avoid any feedback to the hot film. Figure 4.3 gives the structure of the closed-loop scheme with the nearfield-solution.

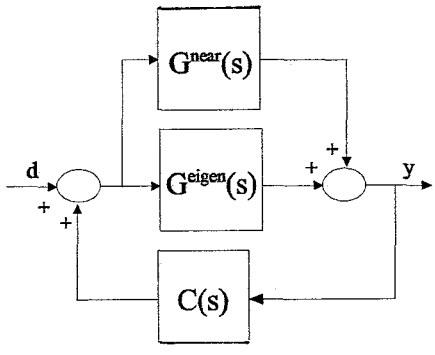

Figure 4.3: Feedback diagram for the eigen- and nearfield-solution

The following closed loop transfer functions can be derived:

$$H^{eigen}_{closedloop}(s) = \frac{Y(s)}{D(s)} = \frac{G^{eigen}(s)}{1 - C(s)G^{eigen}(s)} \tag{4.1}$$

$$H^{eigen+near}_{closedloop}(s) = \frac{Y(s)}{D(s)} = \frac{(G^{eigen}(s) + G^{near}(s))}{1 - C(s)(G^{eigen}(s) + G^{near}(s))} \tag{4.2}$$

To design a controller a classical loop-shaping approach is used. The "loop shape" refers to the magnitude of the loop transfer function $L = G(s)C(s)$ as a function of frequency. For performance (good disturbance attenuation) and stability a large L is required. This implies that the closed loop transfer function will be small. This can be translated in the following demand:

$$\forall\omega \in [\omega_o, \omega_1], \quad \max |H_{closedloop}(i\omega)| \text{ is small} \tag{4.3}$$

The boundary values ω_0 and ω_1 are equal to 314.159 [rad/s] and 942.477 [rad/s] (see Chapter 2).

For disturbances entering at the plant input (often referred to as a load disturbance) a simple proportional controller K yields a good trade-off between output performance and input usage.

$$C(s) = K \tag{4.4}$$

Summarising, the closed loop transfer function has to be minimized in sense of (4.3) for several values of K. To find the optimal values, negative and positive, for the proportional controller first stability and then performance of the closed loop transfer function is studied. To cope with the fractional form of the nearfield-solution the controller will be designed for the eigen-solution. This controller will be used in the system with both solutions and conclusions will be made about the performance.

4.1 Stability

One of the main issues in designing feedback controllers is stability. If the feedback gain is too large, then the controller may 'overreact' and the closed-loop system becomes unstable. To investigate stability the Root-locus method has been used. This method involves the evaluation of the closed-loop poles i.e., the roots of $1 - KG(s)$. The systems are stable if and only if all the closed-loop poles are in the open left hand plane.

The eigen-solution does not have a rational transfer function. If Matlab will be used to calculate the roots an approximation for the time-delay has to be made. For this reason the equation for the roots is solved by hand. The eigen-solution can be represented by a second-order system with dead time. For these systems the following equation is often been used:

$$G(s) = \frac{ae^{-s\tau}}{s^2 + 2\zeta\omega_n s + \omega_n^2} \tag{4.5}$$

To calculate the roots of $1 - KG(s)$ the following equation has to be solved (the method is shown here for negative values of K (For positive K's see appendix A)):

$$1 - (-K)\,G(s) = 0 \tag{4.6}$$

Combining equation (4.6) with (4.5) gives:

$$1 + KG(s) = s^2 + 2\zeta\omega_n s + \omega_n^2 + aKe^{-s\tau} = 0 \tag{4.7}$$

Let $s = i\omega$:

$$-\omega^2 + 2\zeta\omega_n(i\omega) + \omega_n^2 + aKe^{-i\omega\tau} = 0 \tag{4.8}$$

$$K = -\frac{1}{a}((\omega_n^2 - \omega^2) + 2\zeta(i\omega)\omega_n)e^{i\omega\tau} \tag{4.9}$$

Equation (4.9) can be expanded using Eulers formula $e^{i\alpha} = \cos(\alpha) + i\sin(\alpha)$ as:

$$K = -\frac{1}{a}((\omega_n^2 - \omega^2) + 2\zeta(i\omega)\omega_n)(\cos(\omega\tau) + i\sin(\omega\tau)) \tag{4.10}$$

$$K = -\frac{1}{a}\begin{pmatrix} (\omega_n^2 - \omega^2)\cos(\omega\tau) + (\omega_n^2 - \omega^2)i\sin(\omega\tau) + 2\zeta(i\omega)\omega_n(\cos(\omega\tau) \\ -2\zeta\omega\omega_n\sin(\omega\tau) \end{pmatrix}$$

Only the intersections with the imaginary axis (Routh-Hurwitz stability criterion) are of interest:

$$-\frac{1}{a}\left((2\zeta\omega\omega_n)\cos(\omega\tau) + (\omega_n^2 - \omega^2)\sin(\omega\tau)\right) = 0$$

$$\tan(\omega\tau) = \frac{2\zeta\omega\omega_n}{\omega^2 - \omega_n^2} \tag{4.11}$$

Expression (4.11) has been solved graphically. Figure 4.4, gives a representation of both functions, only intersections between the known values for ω are important. The intersection of $\tan(\omega\tau)$ and $\frac{2\zeta\omega\omega_n}{\omega^2-\omega_n^2}$ is found at ω is 713.137[rad/s]

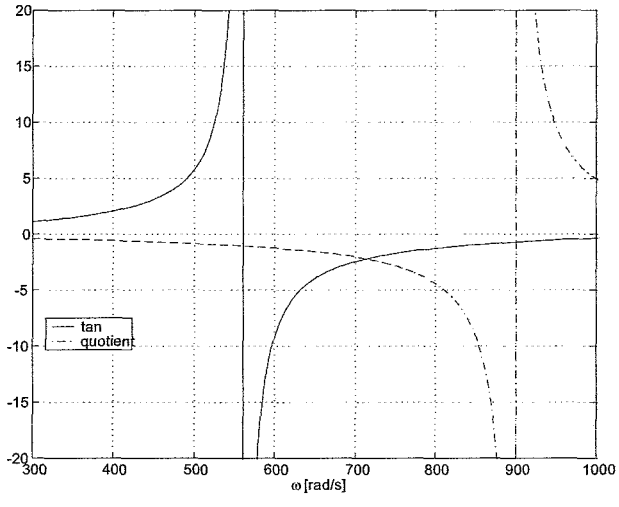

Figure 4.4: Graphical representation of equation (4.12)

therefore K has to be larger than -3.651. Positive values for K have to be smaller than 449. The values for K can be found by solving equation (4.7) using for s 713.137[rad/s] (for the positive value $s = 2062.2$), $\omega_n = 900$[rad/s], $\zeta = 0.52$, $a = 4 \cdot 10^6$ and $\tau = 0.0028$[s]. The values for the undamped natural frequency (ω_n), the damping ratio (ζ), the gain a and the time delay (τ) can be found when equation (3.7) is presented in the form of expression (4.5).

4.2 Performance

The real objective is not to improve stability but improve performance, that is, to make the output y behave in a more desirable manner. A solution has to be found for the optimization problem stated in equation (4.3). This is done by making several Bode-plots of the closed-loop response for different values of K (using the boundaries for K found above and in Appendix A). Eventually the optimal values for K have been found. The positive value for the proportional controller K is 0.815 and the negative value for K is -1.185. From Figure

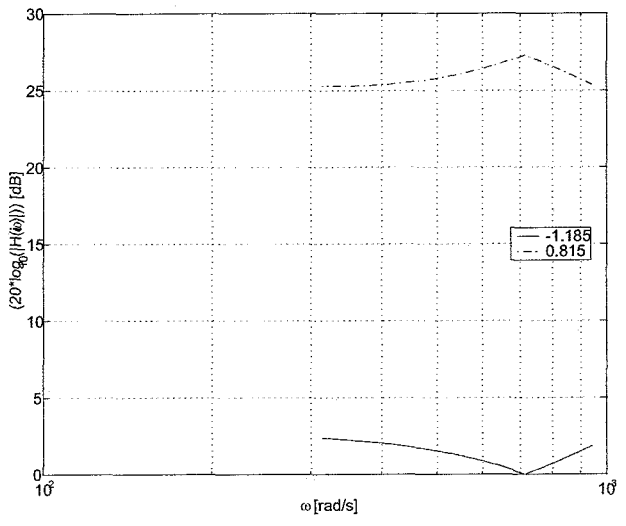

Figure 4.5: Closed loop response for the optimal values of K

4.5 it can be concluded that the magnitude is still larger than one, so there is no disturbance attenuation. Implementing those controllers in the closed-loop transfer funtions with the nearfield-solution gives an even worser result (figure 4.6).

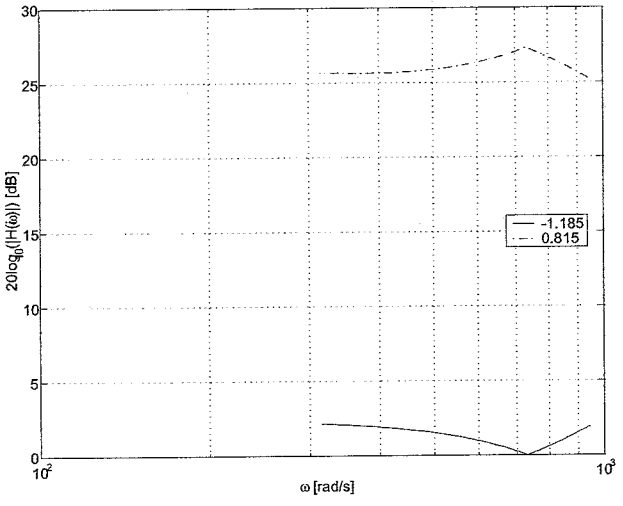

Figure 4.6: Closed loop response for the optimal values of K (with nearfield solution)

Chapter 5

The $\mathcal{H}_\infty$ approach to control design

There are many ways in which feedback design problems can be cast as $\mathcal{H}_\infty$-norm optimization problems. It is very useful therefore to have standard problem formulation into which any particular problem may be transformed. The state-space computation is most convenient to implement on the computer (Matlab). Therefore an appropriate state-space representation for the resulting transfer matrix is necessary.

Let a finite dimensional linear time invariant dynamical system be described by the following linear constant coefficient differential equations:

$$\dot{x} = Ax + Bu, \; x(t_0) = x_0 \tag{5.1}$$

$$y = Cx + Du \tag{5.2}$$

where $x(t) \in \mathsf{R}^n$ is called the system state, $x(t_0)$ is called the initial condition of the system, $u(t) \in \mathsf{R}^m$ is called the system input, and $y(t) \in \mathsf{R}^p$ is the system output. The A, B, C, and D are appropriately dimensioned real constant matrices. Note that the system equations (5.1) and (5.2) can be written in a more compact matrix form:

$$\begin{pmatrix} \dot{x} \\ y \end{pmatrix} = \begin{pmatrix} A & B \\ C & D \end{pmatrix} \begin{pmatrix} x \\ u \end{pmatrix} \tag{5.3}$$

To expedite calculations involving transfer matrices, the following notation is used:

$$\begin{pmatrix} A & B \\ C & D \end{pmatrix} := C(sI - A)^{-1}B + D \tag{5.4}$$

The corresponding transfer matrix from u to y is defined as:

$$Y(s) = G(s)U(s) \tag{5.5}$$

where $U(s)$ and $Y(s)$ are the Laplace transforms of $u(t)$ and $y(t)$ with zero initial condition ($x(0) = 0$). So,

$$G(s) = C(sI - A)^{-1}B + D \tag{5.6}$$

assume that $G(s)$ is a real rational transfer matrix that is proper. The state-space realization is said to be a minimal realization of $G(s)$ if A has the smallest possible dimension (i.e. the fewest number of states). A state-space realization (A, B, C, D) of $G(s)$ is minimal if and only if (A, B) is controllable and (C, A) is observable.

Definition 1 *The dynamical system (5.3) described by the pair (A, B) is said to be* **state controllable** *if, for any initial state $x(0) = x_0$ any $t_1 > 0$, and final state x_1, there exists a (piecewise continuous) input $u(\cdot)$ such that the solution of equation 5.3 satisfies $x(t_1) = x_1$. Otherwise, the system or the pair (A, B) is said to be uncontrollable.*

Definition 2 *The dynamical system described by the pair (C, A) is said to be* **state observable** *if, for any $t_1 > 0$, the initial state $x(0) = x_0$ can be determined from the history of the input $u(t)$ and the output $y(t)$ in the interval of $[0, t_1]$. Otherwise, the system, or the pair (C, A) is said to be unobservable*

5.1 The Background of $\mathcal{H}_\infty$ control

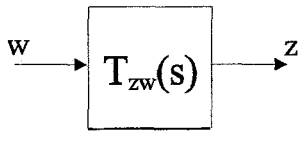

Figure 5.1: Block diagram

Taking the Laplace transform of the system represented in Figure 5.1, it is easy to define the transfer function $T_{zw}(s)$ from $w(s)$ to $z(s)$ (the Laplace transform of w and z), such that

$$z(s) \ , \ T_{zw}(s)\, w(s) = C(sI - A)^{-1} B w(s)$$

Norms of the system transfer function $T_{zw}(s)$ quantify how the system output of interest, z, respond to disturbances w entering the closed-loop system. The expected value of the root mean square (rms) of the output z over the root mean square of the input w for disturbances w of maximally disruptive structure is denoted by the ∞-norm of the system transfer function,

$$\|T_{zw}\|_\infty \ , \ \sup_\omega \bar{\sigma}\left(T_{zw}(i\omega)\right) \leq \gamma$$

where $\bar{\sigma}(\omega)$ is the frequency dependent maximal singular value, viewed as a function of ω, provides more detailed information about the gain characteristics of the system than the $\mathcal{H}_\infty$ norm only. (The $\mathcal{H}_\infty$ norm indicates for an input-output system the maximal gain of the system if the inputs are allowed to vary over the class of signals with bounded 2-norm). γ is an upperbound for the maximum value of the $\mathcal{H}_\infty$ norm for a certain frequency domain.

$\mathcal{H}_\infty$ control is often referred to as "robust" control, as $\|T_{zw}\|_\infty$, reflecting the worst-case amplification of disturbances by the system from the input w

to the output z, is in fact bounded from above by the value of γ used above. Subject to this ∞-norm bound, $\mathcal{H}_\infty$ control minimizes the expected value of the root mean square of the output z over the root mean square of the input w for white Gaussian disturbances w with identity covariance, denoted by the 2-norm of the system transfer function

$$\|T_{zw}\|_2 \ , \ \left(\frac{1}{2\pi}\int_{-\infty}^{\infty} trace\left[T_{zw}\left(i\omega\right) * T_{zw}\left(i\omega\right)\right] d\omega\right)^{1/2}$$

Note that $\|T_{zw}\|_2$ is often cited as a measure of performance of the closed-loop system, whereas $\|T_{zw}\|_\infty$ is often cited as a measure of its robustness.

$\mathcal{H}_2$ control (also known as linear quadratic Gaussian control (LQG)) is an important limiting case of $\mathcal{H}_\infty$ control. It is obtained in the present formulation by relaxing the bound γ on the infinity norm of the closed loop system, taking the limit as $\gamma \longrightarrow \infty$ in the controller formulation. Such a control formulation focuses solely on performance, i.e. minimizing $\|T_{zw}\|_2$. As LQG does not provide any guarantees about system behavior for disturbances of particulary disruptive structure ($\|T_{zw}\|_\infty$), it is often referred to as "optimal" control. Though one might confirm a posteriori that a particular LQG design has favorable robustness properties, such properties are not guaranteed by the LQG control design process. When designing a large number of compensators for an entire array of wavenumbers $\mathrm{Re}\,(\alpha)$ via an automated algorithm, as is necessary in the present problem, it is useful to have a control design tool which inherently builds in system robustness, such as $\mathcal{H}_\infty$. For isolated low-dimensional systems, as often encountered in many industrial processes, a posteriori robustness checks on hand-tuned LQG designs are often sufficient.

The names $\mathcal{H}_2$ and $\mathcal{H}_\infty$ are derived from the system norms $\|T_{zw}\|_2$ and $\|T_{zw}\|_\infty$ which these control theories address, with the symbol $\mathcal{H}$ denoting the particular "Hardy space" in which these transfer function norms are well defined . It deserves mention that the difference between $\|T_{zw}\|_2$ and $\|T_{zw}\|_\infty$ might be expected to be increasingly significant as the dimension of the system is increased. Neglecting, for the moment, the dependence on ω in the definition of the system norms, the matrix Frobenius norms, $(trace\left[T * T\right])^{1/2}$, and the matrix 2-norm, $\bar{\sigma}\left[T\right]$, are "equivalent" up to a constant. Indeed, for scalar systems, these two matrix norms are identical, and for low-dimensional systems, their ratio is bounded by a constant related to the dimension of the system. For high-dimensional discretization of infinite-dimensional systems, however, this norm equivalence is relaxed, and the difference between these two matrix norms may be substantial. The temporal dependence of the two system norms $\|T_{zw}\|_2$ and $\|T_{zw}\|_\infty$ distinguishes them even for low-dimensional systems; the point here is only that, for high dimensional systems, the important differences between these two systems norms is even more pronounced, and control techniques, such as $\mathcal{H}_\infty$, which account for both such norms might prove to be beneficial. Techniques (like $\mathcal{H}_\infty$) which bound $\|T_{zw}\|_\infty$ are especially appropriate for the present problem, as transition from laminar to turbulent is often associated with the triggering of a "worst-case" phenomenon, which is well characterized by this measure. Unfortunately, the ∞-norm of T_{zw} must be sought by an iterative search. The approach used here, suggested by *Doyle et al.* (1989), is

1. guess a value of γ;

2. compute the eigenvalues of the Hamiltonian $H = \begin{pmatrix} A & \frac{1}{\gamma^2}BB \\ -CC & -A \end{pmatrix}$;

3. $\|T_{zw}\|_\infty < \gamma$ if H has no eigenvalues on the imaginary axis and $H \in dom\,(Ric)$ (See Doyle et al. 1989 for definition of the latter property.) Thus, we may increase or decrease accordingly, using a golden section search, and repeat from 2. until bounds on $\|T_{zw}\|_\infty$ reach a desired tolerance.

5.2 $\mathcal{H}_\infty$ control for this problem

Consider the general control configuration as given in Figure 5.2.P describes the

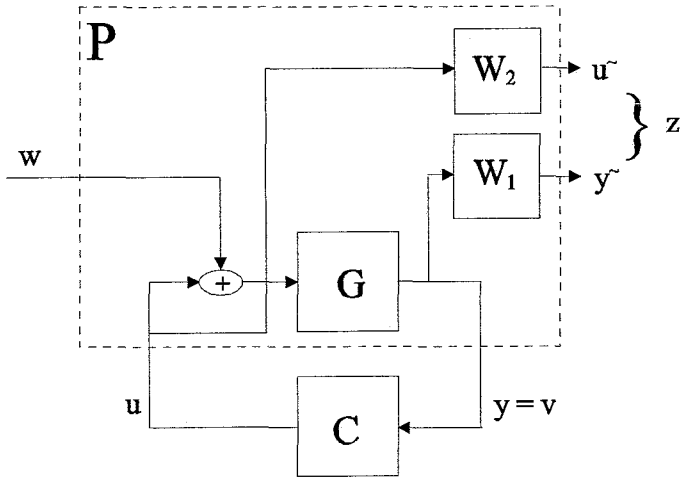

Figure 5.2: General control configuration

augmented plant containing beyond the process model, all the filters for characterizing the inputs and weighting the penalized outputs, w are the exogenous inputs (commands, disturbance and noise (in this case only disturbance)), z are the exogenous outputs ("error"signals to be minimized), v are the controller inputs (measured plant outputs, measured disturbances etc.) and u are the control signals.

The $\mathcal{H}_\infty$-control problem is formalized as follows: Synthesize a stabilizing controller C such that $\|T_{zw}(P,C)\|_\infty < \gamma$. The ultimate aim is to minimize the $\mathcal{H}_\infty$-norm of the closed-loop transfer function. Therefore an admissible C has to be synthesized for γ as small as possible. Admissible controllers are all linear time-invariant systems K that internally stabilize the configuration of Figure 5.1 .

The structure of Figure 5.2 has been built in Matlab using the μ-Analysis and Synthesis Toolbox. The blocks W_1 and W_2 are weighting filters. Our only interest is to cancel the waves in a given domain for ω (Chapter 2). Therefore the control signal u and the output y are weighed in this domain using almost ideal bandpass filters. These filters are based on a fourth-order Butterworth

filter. The augmented plant P is described by the matrices A ($[A_1, A_2]$) (A is a (10×10)-matrix, for lay-out reasons it is split-up in two parts) , B, C and D.

$$A_1 = \begin{pmatrix} -9.3 \cdot 10^2 & -6.3 \cdot 10^3 & 0 & 0 & 0 \\ 1.3 \cdot 10^2 & 0 & 0 & 0 & 0 \\ 0 & 2 \cdot 10^3 & -8.9 \cdot 10^2 & -1.2 \cdot 10^2 & -1.0 \cdot 10^3 \\ 0 & 0 & 8.2 \cdot 10^3 & 0 & 0 \\ 0 & 0 & 0 & 32 & 0 \\ 0 & 0 & 0 & 0 & 64 \\ 0 & 0 & 0 & 0 & 0 \\ 0 & 0 & 0 & 0 & 0 \\ 0 & 0 & 0 & 0 & 0 \\ 0 & 0 & 0 & 0 & 0 \end{pmatrix}$$

$$A_2 = \begin{pmatrix} 0 & 0 & 0 & 0 & 0 \\ 0 & 0 & 0 & 0 & 0 \\ -5.2 \cdot 10^3 & 0 & 0 & 0 & 0 \\ 0 & 0 & 0 & 0 & 0 \\ 0 & 0 & 0 & 0 & 0 \\ 0 & 0 & 0 & 0 & 0 \\ 0 & -8.9 \cdot 10^2 & -1.2 \cdot 10^2 & -1.0 \cdot 10^3 & -5.2 \cdot 10^3 \\ 0 & 8.2 \cdot 10^3 & 0 & 0 & 0 \\ 0 & 0 & 32 & 0 & 0 \\ 0 & 0 & 0 & 64 & 0 \end{pmatrix}$$

$$B = \begin{pmatrix} 1.3 \cdot 10^2 & 0 & 0 & 0 & 0 & 0 & 0 & 0 & 0 & 0 \\ 1.3 \cdot 10^2 & 0 & 0 & 0 & 0 & 0 & 4 & 0 & 0 & 0 \end{pmatrix}^T$$

$$C = \begin{pmatrix} 0 & 0 & 0 & 0 & 0 & 0 & 0 & 0 & 0 & 0 \\ 0 & 0 & 0 & 24 & 0 & 0 & 0 & 0 & 0 & 0 \\ 0 & 0 & 0 & 0 & 0 & 0 & 0 & 12 & 0 & 0 \\ 0 & 2.4 \cdot 10^2 & 0 & 0 & 0 & 0 & 0 & 0 & 0 & 0 \end{pmatrix}$$

$$D = \begin{pmatrix} D_{11} & D_{12} \\ D_{21} & D_{22} \end{pmatrix} = \begin{pmatrix} 1 & 1 \\ 0 & 0 \\ 0 & 0 \\ 0 & 0 \end{pmatrix}$$

The expressions for A, B, C and D have found by first making a realization of equation (3.7) in state space notation using equation (5.6), then the weighting filters added using the routine (*sysic.m*) in the μ-Analysis and Synthesis Toolbox to form interconnections for system matrices.

This makes it possible to let the algorithm of *Doyle et. al.* calcute a controller, unfortunately using the μ-Analysis and Synthesis Toolbox, this is not possible, because D_{21} does not have full rank. It means that not all measurements are polluted by "noise", i.e. the disturbance. (The problem can be solved by investigating whether the problem definition is realistic and some measurement noise should be added or fooling the algorithm by giving D_{21} a very small value). In this case another method is used to find a (sub)optimal controller, because the objective was only to show if closed-loop control is possible

5.3 LMI-synthesis

This method is based on Linear matrix inequalities (LMIs). This technique is fast, simple and at the same time a most reliable and efficient way to synthesize $\mathcal{H}_\infty$-controllers. This section is organized as follows. In the next subsection the LMIs are introduced, then is shown how the synthesis question is considered how to obtain a controller which stabilize a given dynamical system so as to minimize the $\mathcal{H}_\infty$-norm of the closed loop system.

5.3.1 Standard problems involving LMIs

The basic idea of the LMI method is to formulate a given problem as an optimization problem with linear objective and linear matrix inequality constraints. An LMI constraint on a vector $x \in \mathsf{R}^m$ is one of the form:

$$F(x) = F_0 + \sum_{i=1}^{m} x_i F_i > 0$$

where the symmetric matrices $F_i = F_i^T \in \mathsf{R}^{nxn}$, $i = 0, ..., m$ are given. The set $\{x|F(x) > 0\}$ is convex, and need not to have a smooth boundary.

5.3.2 Synthesis of the $\mathcal{H}_\infty$-controller

The same construction for the augmented plant can be used as derived above. Only the algorithm used to synthesize a controller will be different. In Matlab the LMI Control Toolbox has been used. The LMI Control Toolbox supports continuous and discrete time $\mathcal{H}_\infty$ synthesis using either Ricatti- or LMI based approaches. Both approaches are based on state space calculations. LMI synthesis routines have no assumptions on the matrices which define the system, [2]. A similar approach as in Chapter 4 is used to find a controller, because no approximations for time delay or fractional terms will be made. First a controller is calculated for the eigen-solution without the time-delay. This controller is implemented in a system with the dead time and the nearfield solution. Figure 5.3 gives a Bode-plot of the closed-loop and loop transfer function. As expected the nearfield influences are very small. A ninth order controller is built with the following state space representation:

$$C = \begin{pmatrix} A_c & C_c \\ B_c & D_c \end{pmatrix}$$

where $(A = ([A_{c_1}, A_{c_2}])$ (A is a (9×9)-matrix, for lay-out reasons it is split-up in two parts):

$$A_{c_1} = \begin{pmatrix} 8.1 \cdot 10^5 & -2.2 \cdot 10^2 & -1.1 \cdot 10^4 & -6.8 \cdot 10^6 & -5.6 \cdot 10^9 \\ 4.2 \cdot 10^6 & 0 & 0 & 0 & 0 \\ 0 & 32 & 0 & 0 & 0 \\ 0 & 0 & 1 & 0 & 0 \\ 0 & 0 & 0 & 1 & 0 \\ 0 & 0 & 0 & 0 & 1 \\ 0 & 0 & 0 & 0 & 0 \\ 0 & 0 & 0 & 0 & 0 \\ 0 & 0 & 0 & 0 & 0 \end{pmatrix}$$

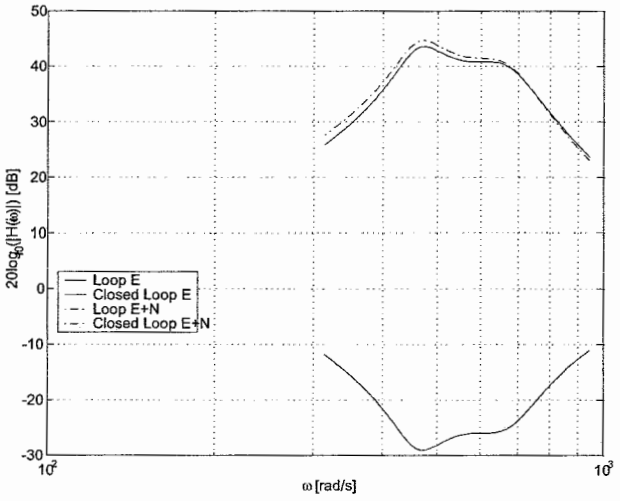

Figure 5.3: Bode-plot of the closed-loop and loop transfer function

$$A_{c_2} = \begin{pmatrix} -2.0 \cdot 10^{12} & -9.6 \cdot 10^{14} & -1.6 \cdot 10^{17} & -4.5 \cdot 10^{19} \\ 0 & 0 & 0 & 0 \\ 0 & 0 & 0 & 0 \\ 0 & 0 & 0 & 0 \\ 0 & 0 & 0 & 0 \\ 0 & 0 & 0 & 0 \\ 1 & 0 & 0 & 0 \\ 0 & 1 & 0 & 0 \\ 0 & 0 & 1 & 0 \end{pmatrix}$$

$$B_c = \begin{pmatrix} 2.9e \cdot 10^{-3} & 7.9 \cdot 10^{-7} & 4.0 \cdot 10^{-5} & 0.025 & 200 & 7.1 \cdot 10^{3} & 3.5 \cdot 10^{6} & 5.9 \cdot 10^{8} & 1.6 \cdot 10^{11} \end{pmatrix}$$

$$C_c = \begin{pmatrix} 1.4 \cdot 10^{11} & 0 & 0 & 0 & 0 & 0 & 0 & 0 & 0 \end{pmatrix}^T$$

$$D_c = -5.0 \cdot 10^{-2}$$

For performance (good disturbance attenuation) and stability a large loop transfer function is required. A large loop transfer function implies that the closed loop transfer function has to be small (Chapter 4).The straight line and the dashed-dotted line in Figure 5.3 in the region with a magnitude larger than zero give the loop transfer function ($G(s)C(s)$) for the eigen-solution and the eigensolution combined with the nearfield solution. The lines in the region with a magnitude less than zero gives the closed-loop response of the system. The dashed-dotted line lies under the straight line. This was expected because the

distance chosen between the actuator and sensor would avoid any feedback from the upstream nearfield solution. From Figure 5.3 can be concluded that the loop transfer function is large and the closed loop transfer function is small, so it has to be possible to control disturbances (instabilities) in the boundary layer using feedback control.

Chapter 6

Conclusion and Recommendations

6.1 Conclusion

The problem is to synthesize a closed-loop controller for a fluid flowing past a flat plate. Therefore first some insight has been given in fluid dynamics. Secondly it is tried to derive a model, first using a transfer function analysis and later using the theory of fractional terms. Unfortunately the second method will not give a proper model to work with. Then a controller is derived using classical control methods. Unfortunately this problem deals with time delay so no use can be made of the routines in Matlab. This proportional controller does not reach the performance demand. Therefore a new controller has been build using $\mathcal{H}_\infty$-control theory. First the algorithm stated by *Doyle et al, [7].* is used. But this algorithm has an assumption which restricts the use in this case. Secondly Linear Matrix Inequalities (LMIs) are used to synthesize a controller. The resulting ninth-order controller reaches the performance demand, $\forall\omega \in [\omega_o, \omega_1]$, $\max|H_{closedloop}(i\omega)|$ is small, (small is in this case of disturbance attentuation less than zero) so it is possible to construct a closed-loop controller for this problem.

6.2 Recommendations

- Validation of the controller numerically or experimentally, because in theory it seems possible to use feedback control to delay transition from a laminar to a turbulent boundary layer. Only after validation a valid judgement can be made;
- If a ninth order controller gives problems by implementing it in the real world, the controller could be reduced using techniques like truncation;
- The use of fractional terms in control engineering is a relatively new thought. In this project is not only dealt with fractional terms but also with time delay. Research has to be done on such systems.

Bibliography

[1] Bewley, T.R.; *Flow control: new challenges for a new Renaissance* (2001); Progress in Aerospace Sciences, vol. 37, pp. 21-58

[2] Boyd, S., El Ghaoui, L., Feron, E., Balakrishnan, V.; *Linear Matrix Inequalities in systems and control theory* (1994); Society for Industrial and Applied Mathematics (SIAM) Philadelphia (book)

[3] Chen, B.M.; *Robust and $\mathcal{H}_\infty$-control* (2000); Springer London (book)

[4] Clark, R.N.; *Control system dynamics* (1996); Cambridge University Press, New York (book)

[5] Damen, A. and Weiland, S.; *Robust Control* (2001); Technische Universiteit Eindhoven (lecture notes)

[6] Dorf R.C.; Modern Control Systems (1989); fifth edition; Addison-Wesley Publishing Company, New York (book)

[7] Doyle, J.C., Francis, B., and Tannenbaum, A.; *Feedback Control Theory* (1992); Macmillam Publishing Company (book)

[8] Franklin, G.F., Powell, J.D. and Emami-Naeini, A.; *Feedback control of dynamic systems* (1994); third edition; Addison-Wesley Publishing Company, New York (book)

[9] Fingerson, L.M. and Freymuth, P.; *Thermal Anemometers* in *Fluid Mechanics Measurement: Second Edition* (1996) pp. 115-174; Goldstein R.J.; Taylor & Francis, Washington (book)

[10] Fridman, E. and Shaked, U.; *A Descriptor System Approach to $\mathcal{H}_\infty$ Control of Linear Time-Delay System* (2002); IEEE Trans. Autom. Control, vol. 47, no. 2, pp. 253-270

[11] Gaster, M.; *Active control of boundary layer instabilities using MEMs* (2000); Reprint from Current Science, vol. 79, no. 6, pp. 774-780

[12] Ghaoui El, L.; *Advances in Linear Matrix Inequalities methods in Control* (2000); SIAM Philadelphia (book)

[13] Hwang, C., Leu, J.F., Tsay, S.Y.; *A Note on Time-Domain Simulations of Feedback Fractional-Order Systems* (2002); IEEE Trans. Autom. Control, vol. 47, no. 4, pp. 625-631

[14] Jeung, E.T., Kwon, S.H., Kim, J.H., Park, H.B.; *An LMI Approach to $\mathcal{H}_\infty$ Control for Linear Delay Systems* (1998); Proc. of the American Control Conference, Philadelphia, pp. 2398-2402

[15] Loiseau, J.J. and Mounier, H.; *Stabilisation de l'équation de la chaleur commandée en flux* (1998); ESIAM: Proceedings , vol. 5, pp. 131-144

[16] Lunze, J.; *Robust multivariable feedback control* (1988); Prentice-Hall International Limited, London (book)

[17] Marshall, J.E.; *Control of time-delay systems* (1979); The Institution of Electrical Engineers, London (book)

[18] Meinsma, G. and Zwart, H.; *On $\mathcal{H}_\infty$ Control for Dead-Time Systems (2000);* IEEE Trans. Autom. Control, vol. 45, no. 2, pp. 272-285

[19] Nagrath I.J. and Gopal M.; *Control Systems Engineering: Second Edition* (1986); John Wiley & Sons, Singapore (book)

[20] Podlubny, I.; *Fractional Differential Equations* (1999); Academic Press, San Diego (book)

[21] Sabersky, R.H., Acosta, A.J., Hauptmann, E.G., Gates, E.M.; *Fluid flow: a first course in fluid mechanics* (1999); fourth edition; Prentice-Hall, New Jersey (book)

[22] Sánchez-Peña, R.S., Sznaier M.; *Robust Systems: Theory and Applications* (1998); John Wiley & Sons, New York (book)

[23] Schlichting, H.; *Boundary Layer theory* (1979); McGraw-Hill Inc., New York (book)

[24] Shaikh, F.N, Gaster, M.; *Receptivity to free-stream disturbances* (1996); Engineering Department Queen Mary University (report)

[25] Skogestad, S., Postlethwaite. I.; *Multivariable Feedback Control: Analysis and Design* (1996); John Wiley & Sons, New York (book)

[26] Vegte van de J.; *Feedback Control systems* (1986); Prentice-Hall International Inc., London (book)

[27] Zhou, K. with Doyle J.C. and Glover K.; *Robust and Optimal Control (*1996); Prentice-Hall Inc., New Jersey (book)

[28] Zhou, K. with Doyle J.C.; *Essentials of Robust Control: International Edition* (1998); Prentice-Hall International Limited, London (book)

A: Roots for positive values of K

To calculate the roots of $1 - L(s)$ for positive values of K the following equation has to be solved:

$$1 - L(s) = 0 \tag{A.1}$$

$$1 - C(s)G(s) = 1 - KG(s) = 0 \tag{A.2}$$

Combining equation (A.2) with (4.5) gives:

$$1 - KG(s) = s^2 + 2\zeta\omega_n s + \omega_n^2 - aKe^{-s\tau} = 0$$

Let $s = i\omega$:

$$-\omega^2 + 2\zeta\omega_n(i\omega) + \omega_n^2 - aKe^{-i\omega\tau} = 0 \tag{A.3}$$

$$K = \frac{1}{a}((\omega_n^2 - \omega^2) + 2\zeta(i\omega)\omega_n)e^{i\omega\tau} \tag{A.4}$$

Equation (A.4) can be expanded using Eulers formula $e^{i\alpha} = \cos(\alpha) + i\sin(\alpha)$ as:

$$K = \frac{1}{a}((\omega_n^2 - \omega^2) + 2\zeta(i\omega)\omega_n)(\cos(\omega\tau) + i\sin(\omega\tau)) \tag{A.5}$$

$$K = \frac{1}{a}\left(\begin{array}{c} (\omega_n^2 - \omega^2)\cos(\omega\tau) + (\omega_n^2 - \omega^2)i\sin(\omega\tau) + 2\zeta(i\omega)\omega_n(\cos(\omega\tau) \\ -2\zeta\omega\omega_n\sin(\omega\tau) \end{array} \right)$$

Only the intersections with the imaginary axis (Routh-Hurwitz stability criterion) are of interest:

$$\Im(K) = 0$$

$$\frac{1}{a}\left((2\zeta\omega\omega_n)\cos(\omega\tau) + (\omega_n^2 - \omega^2)\sin(\omega\tau)\right) = 0$$

$$\tan(\omega\tau) = -\frac{2\zeta\omega\omega_n}{\omega^2 - \omega_n^2} \tag{A.6}$$

Expression (A.6) has been solved graphically. Figure 1, gives a representation of both functions, only intersections between $\omega = [314.159, 942.477]$ are important. ω_n has a value of 900 [rad/s], τ is 0.0028 and ζ has a value of 0.5175.

There are no intersection in the domain for ω. The first intersection is found at 0 and one at 2062.2 [rad/s], values for K will be 0.2025 and 495 respectively.

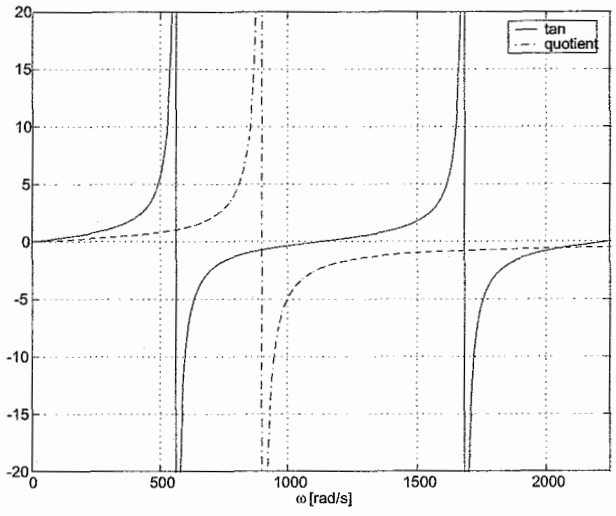

Figure 1: Graphical representation of equation (A.6)

Summary

On wings of aircrafts transition from a laminar to a turbulent boundary layer generally occur through the amplification of naturally excited instability waves. These waves are caused by acoustic or vorticity fluctuations. These fluctuations are caused by roughness elements on the wing. Research has been done for a long time to find out how the transition from laminar to turbulent takes place and how it can be controlled. The instability waves can be cancelled passive or active. In this report an investigation has been done if it is possible to cancel the waves actively using feedback-control.

In chapter 2 is tried to derive a model for the transition. This is done using the Navier-Stokes-equation resulting in an equation, which describes the stability of the system. This equation is called the Orr-Sommerfeld equation. Unfortunately it is not possible to find a nice solution for the Orr-Sommerfeld equation. So another manner of deriving a model is used in chapter 3. The method used is called transfer function analysis. In this method numerical data (derived by Yong Li) is plotted in a Bode-plot. Then is tried to fit lines with a prescribed slope to it. Unfortunately it is not possible to get a good resemblance using this lines, so other slopes are tried. This results in a model with fractional terms.

In chapter 4 a proportional controller is synthesized for this system, using the Routh-stability criterium and a performance aim. This controller will not take the performance aim. So a controller has to be synthesized using a more modern manner, namely $\mathcal{H}_\infty$-theory. The controller can eventually in chapter 5 be synthesized using Linear Matrix Inequalities. This controller fullfils the performance aim. Eventually conclusion are drawn and recommendations are madei n chapter 6.

Samenvatting

Op vleugels van vliegtuigen vindt omzetting van een laminaire naar turbulente grenslaag plaats door de versterking van natuurlijke verstoringen. Deze verstoringen worden veroorzaakt door akoestische of vorticitietsfluctuaties. Deze fluctuaties worden veroorzaakt door oneffenheden op de vleugel. Er wordt al een lange tijd onderzoek gedaan naar hoe de omzetting van laminair naar turbulent plaatsvindt en naar het onderdrukken van de verstoringen. Deze verstoringen kunnen passief of actief onderdrukt worden. In dit verslag wordt gekeken of het mogelijk is om deze verstoringen actief te onderdrukken gebruik makend van 'feedback'-regelstrategieën.

In hoofdstuk 2 wordt getracht meer inzicht, op een wiskundige manier, te geven hoe deze verstoringen ontstaan. Met behulp van de Navier-Stokes equation wordt uiteindelijk een vergelijking afgeleid die de stabiliteit van het systeem beschrijft. Deze vergelijking wordt de Orr-Sommerfeld vergelijking genoemd. Helaas is het niet mogelijk om een nette oplossing voor deze vergelijking te vinden, dit wordt o.a. veroorzaakt doordat de verstoringen aangroeien in de tijd, dus zal er in het constueren van de regelaar rekening gehouden moeten worden met tijdsvertraging.

In hoofdstuk 3 wordt door een overdrachtsfunctie-analyse een model afgeleidt voor het probleem. Bij de overdrachtsfunctie-analyse is in een Bode-grafiek wordt getracht de numerieke data (verkregen uit promotie-onderzoek van Yong Li) te benaderen met lijnen met een voorgeschreven steilheid. Helaas geven deze lijnen niet een perfecte benadering zodat uitgeweken wordt naar fractionele termen. Uiteindelijk is het toch mogelijk op een model af te leiden.

In hoofdstuk 4 is getracht een proportionele regelaar te maken voor dit systeem. Hierbij is gebruik gemaakt van het Routh-criterium voor stabiliteit en een eis aan de prestatie. Het is niet mogelijk om met een proportionele regelaar aan de prestatie-eis te voldoen, zodat de regelaar op een andere manier geconstrueerd zal moeten worden. Dit gebeurd in hoofdstuk 5 met behulp van $\mathcal{H}_\infty$-theorie. De regelaar wordt bepaald met de methoden van lineare matrix ongelijkheden. Deze regelaar blijkt wel aan de prestatie-eis te kunnen voldoen, waarop uiteindelijk in hoofdstuk 6 de conclusies en aanbevelingen volgen.